

SCIENTIFIC REPORTS



OPEN

Anchorage of Au³⁺ into Modified Isoreticular Metal–Organic Framework-3 as a Heterogeneous Catalyst for the Synthesis of Propargylamines

Lili Liu, Xishi Tai, Xiaojing Zhou, Chunling Xin & Yongmei Yan

Postsynthetic modification of metal-organic framework is a general and practical approach to access MOF-based catalysts bearing multiple active sites. The iso-reticular metal-organic framework-3 (IRMOF-3) was modified with lactic acid through condensation reaction of the carboxyl group of lactic acid and amino group present in IRMOF-3 frameworks. Au³⁺ was subsequently anchored onto the metal-organic framework IRMOF-3 using postsynthetic modification. The synthesized IRMOF-3-LA-Au (LA = lactic acid) was characterized by powder X-ray diffraction, N₂ adsorption-desorption, infrared spectroscopy, liquid-state nuclear magnetic resonance, thermogravimetric analysis, H₂-temperature programmed reduction, transmission electron microscopy, and inductively coupled plasma-optical emission spectrometry. IRMOF-3-LA-Au acted as an efficient heterogeneous catalyst in the synthesis of propargylamines by three-component coupling reaction of aldehyde, alkyne, and amine. Moreover, the catalyst is applicable to various substituted substrates, including aromatic and aliphatic aldehydes, alkyl- and aryl-substituted terminal alkynes, and alicyclic amines. In addition, the catalyst can be easily separated from the mixture and can be reused for four consecutive cycles.

The design and synthesis of novel molecular scaffolds with unique structural and biological properties is an interesting challenge^{1,2}. Propargylamines exhibit biological properties, such as anti-Alzheimer, anti-Parkinsonian, and antidepressant activities^{3–5}. Methods used to prepare propargylamines include amination of propargylic electrophiles⁶, nucleophilic addition of alkynes to imines or enamines⁷, and three-component (aldehyde, terminal alkyne, and amine, A³) coupling reactions through C–H activation^{8,9}. Among these synthetic strategies, A³ coupling is the most efficient, and it permits construction of complex structures from simple starting materials with water as byproduct^{10,11}. In recent years, various metals such as Au⁹, Cu⁸, Ag¹², In¹³, Fe¹⁴, Zn¹⁵, and Ni¹⁶ were extensively used to synthesize propargylamines. Among these metals, cationic gold species have received special attention because of their effective catalytic activity in A³ coupling reactions^{17,18}. Development of efficient, environmentally friendly, and economical catalysts to synthesis of propargylamines has become more important in green and sustainable development in the chemical industry. Homogeneous catalysts have many attractive properties, such as high activities and selectivities. However, many homogeneous catalytic systems cannot be commercialized because of difficulties associated with separating the products from the catalyst¹⁹. Heterogeneous catalysts often have lower activity or selectivity but can be easily reused. The recent researches had shown that metal-organic frameworks (MOFs) could bridge the gap between homogeneous and heterogeneous catalysis^{20,21}.

MOFs are a relatively new class of inorganic-organic hybrid materials, which have tremendously attracted interest due to their potential applications in gas storage and adsorption^{22,23}, molecular separation^{24,25}, fluorescence^{26,27}, and sensors^{28,29}. Moreover, MOFs have aroused interest in heterogeneous catalysis owing to their high surface areas, uniform pores, and chemical tunability^{30,31}. Postsynthetic modification of MOFs has recently been employed as a general approach for incorporating a wide range of functional groups into MOFs^{32–37}. Topologically diverse

School of Chemistry & Chemical Engineering and Environmental Engineering, Weifang University, Weifang, 261061, China. Correspondence and requests for materials should be addressed to L.L. (email: liulili122@wfu.edu.cn) or X.T. (email: taix@wfu.edu.cn)

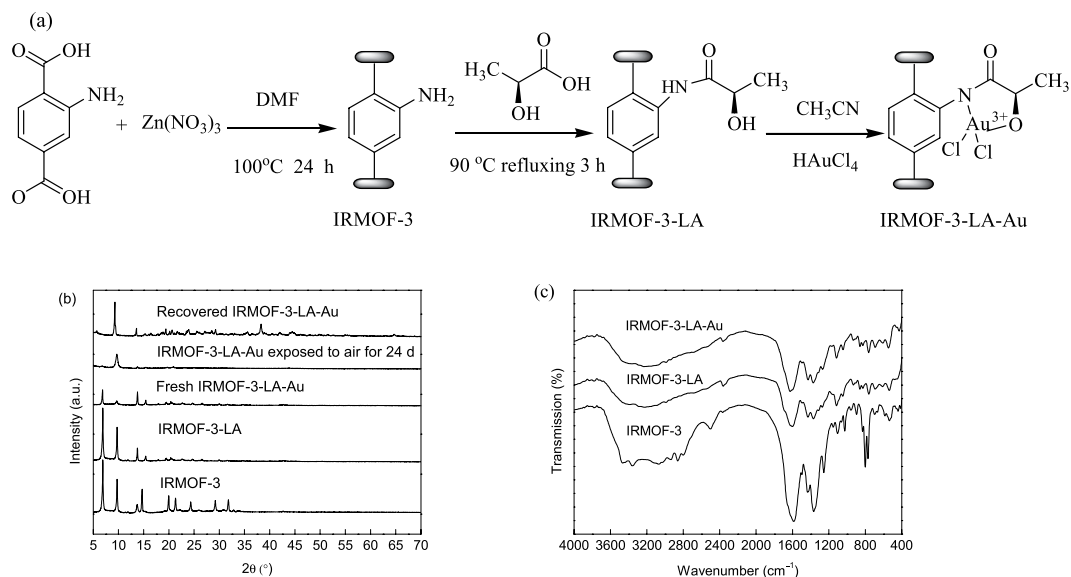


Figure 1. (a) Procedure for obtaining the Au^{3+} -containing catalyst IRMOF-3-LA-Au, (b) X-ray diffraction patterns of IRMOF-3, IRMOF-3-LA, IRMOF-3-LA-Au, and recovered IRMOF-3-LA-Au (c) IR spectrum of as-synthesized IRMOF-3, IRMOF-3-LA, and IRMOF-3-LA-Au.

MOFs can be customized by postsynthetic modification with different functional groups^{38–42}. Wittmann *et al.*⁴² synthesized the remarkable stabilisation of the mesoporous MOF Al-MIL-101-NH₂ by postsynthetic modification with phenyl isocyanate. Moreover, UMCM-1-NH₂ was modified with two metal-binding groups that were metallated with Fe^{3+} and Cu^{2+} to yield UMCM-1-AMFesal and UMCM-1-AMCupz, respectively³³. UMCM-1-AMFesal is catalytically active in Mukaiyama–aldol reaction over multiple catalytic cycles without showing loss of activity or crystallinity³³. Gee *et al.*³⁵ prepared DMOF-1-NHak through postsynthetic modification using diketene. Candu *et al.*⁴³ prepared a highly active and enantioselective MOF through postsynthetic modification of $[\text{Cu}_2(\text{mand})_2(\text{hmt})]$ (mand = mandelic acid, hmt = hexamethylenetetramine) with chiral and dimeric Cr^{3+} salen complexes. Tabatabaeian *et al.*⁴⁴ designed a novel heterogeneous catalyst for oxidation reactions by anchoring a Ru Schiff base moiety onto microporous isorecticular metal–organic framework-3 (IRMOF-3) via postsynthetic method. The catalyst shows high activity toward selective oxidation of arenes and heteroaromatic compounds and for oxidation of sulfids to sulfoxides and sulfones.

In the present study, we designed and synthesized a new Au^{3+} -containing catalyst, IRMOF-3-LA-Au, through postsynthetic modification of IRMOF-3 with lactic acid. IRMOF-3-LA-Au was found to be active and selective for catalyzing A^3 coupling reaction of aldehyde, alkyne, and amine in 1,4-dioxane. They display better catalytic activity than the catalyst containing Au^0 nanoparticles. Furthermore, the catalyst is compatible with various substituted substrates and could be reused for at least four reaction cycles.

Results and Discussion

Synthesis and Characterization. The condensation of the amine-functionalized framework IRMOF-3 and salicylaldehyde has been reported in our previously study¹⁷. The present study investigated the ability of lactic acid to modify IRMOF-3 and generate a new functionalized MOF IRMOF-3-LA in a parallel approximation. The functionalized IRMOF-3-LA was treated with HAuCl_4 to generate the Au^{3+} -containing catalyst IRMOF-3-LA-Au. Figure 1a shows the synthesis pathway in the functionalized MOF system. IRMOF-3 was synthesized via a solvothermal method at 100 °C for 24 h by using 2-aminoterephthalic acid, $\text{Zn}(\text{NO}_3)_2 \cdot 6\text{H}_2\text{O}$, and *N,N'*-dimethylformamide (DMF). The as-synthesized IRMOF-3 was washed with DMF and CHCl_3 prior to postsynthetic modification to remove the unreacted 2-aminoterephthalic acid. IRMOF-3-LA was obtained via treatment with lactic acid in a 1:3.5 ratio in refluxing CH_3CN for 3 h through condensation reaction of the carboxyl group of lactic acid and amino group present in IRMOF-3 frameworks. As shown in Fig. 1a, hydroxyl groups were successfully grafted onto IRMOF-3, and amide groups formed. The hydroxyl and amide groups of the resulting IRMOF-3-LA were used as anchoring groups to stabilize the Au^{3+} ions. The functionalized IRMOF-3-LA was subsequently treated with HAuCl_4 to generate the Au^{3+} -containing IRMOF-3-LA-Au catalyst.

The XRD patterns of IRMOF-3, IRMOF-3-LA, and IRMOF-3-LA-Au are compared in Fig. 1b. The powder X-ray diffraction (PXRD) spectra of IRMOF-3 prepared by the solvothermal method matched well with those reported results^{36,45}. The cubic lattice of IRMOF-3 is well retained even after modification with lactic acid and HAuCl_4 . During the course of these investigations, IRMOF-3-LA-Au was observed to decompose in air. The XRD pattern of the sample changed significantly after exposure to air for 24 day. The intensity of the peak at $2\theta = 6.8^\circ$ decreased severely in XRD pattern. Joseph *et al.* reported that the reflections in XRD pattern for IRMOF-3 decrease over time after exposing to ambient air for 4 days⁴⁶. The change in XRD patterns can be attributed to atmospheric water^{47,48}. The peak centered at $2\theta = 6.8^\circ$ disappeared for IRMOF-3-LA-Au after four

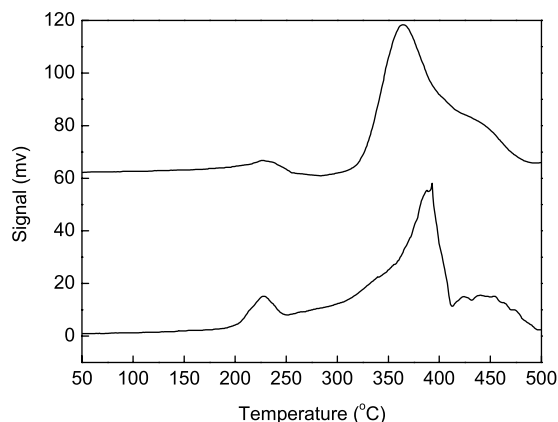


Figure 2. H_2 -TPR profiles characterizing the reduction temperature of Au^{3+} stabilized by metal-organic framework. (a) IRMOF-3-LA-Au (50 mg); (b) Recovered IRMOF-3-LA-Au after four cycles of A^3 coupling reactions at $80\text{ }^\circ\text{C}$ (50 mg).

runs, suggesting that the structure of IRMOF-3 decomposed during A^3 coupling reaction. Notably, in the XRD pattern of recovered IRMOF-3-LA-Au, the $Au(111)$, $Au(200)$, and $Au(220)$ peaks were observed at $2\theta = 38.3^\circ$, 44.5° , and 64.7° , respectively (JCPDS 7440-57-5). IRMOF-3, IRMOF-3-LA-Au, and recovered IRMOF-3-LA-Au exhibited type I isotherms at 77 K (Figure S1). The nitrogen sorption study revealed that the BET surface area and pore volume of IRMOF-3 were $1212\text{ m}^2/\text{g}$ and $0.46\text{ cm}^3/\text{g}$, respectively. After modification with lactic acid and gold, IRMOF-3-LA-Au showed a BET surface area of $687\text{ m}^2/\text{g}$ with a pore volume of $0.38\text{ cm}^3/\text{g}$. The surface area and pore volume of IRMOF-3-LA-Au were smaller than those of IRMOF-3. This characteristic likely resulted from the presence of lactic acid and gold in the pores of the catalyst. Recovered IRMOF-3-LA-Au showed a severely decrease in the BET surface area ($32\text{ m}^2/\text{g}$) and pore volume ($0.01\text{ cm}^3/\text{g}$) as a result of the decomposition of IRMOF-3 during A^3 coupling reaction. IR spectroscopy was used to characterize the functional groups in IRMOF-3, IRMOF-3-LA, and IRMOF-3-LA-Au. Bands at 3473 and 3356 cm^{-1} correspond with the asymmetric and symmetric stretching vibrations of $-\text{NH}_2$ of the NH_2 -BDC ligand, which demonstrates that the amino groups are free in the as-synthesized IRMOF-3^{17,49}. In addition, a peak can be observed at 800 cm^{-1} , which was assigned to the wagging vibration of $-\text{NH}_2$ of the NH_2 -BDC ligand. The IRMOF-3 also displayed bands at 1591 , 1361 , and 1257 cm^{-1} , and these bands correspond to the $\text{C}=\text{C}$ in the benzene ring, $\text{C}-\text{N}$, and $\text{C}-\text{O}$ vibration⁵⁰. After modification with lactic acid and gold, noticeable changes were observed at 3500 – 3200 cm^{-1} . The $-\text{NH}_2$ bands at 3473 and 3356 cm^{-1} notably weakened in IRMOF-3-LA and IRMOF-3-LA-Au samples. Furthermore, the band at 800 cm^{-1} , which is assigned to the wagging vibration of $-\text{NH}_2$, was disappeared after reaction with lactic acid. This indicated that the carboxyl group of lactic acid had reacted with amino group present in the frameworks of IRMOF-3. $^1\text{H-NMR}$ analysis was further used to determine the percentage of linker functionalization by lactic acid (Figure S2). $^1\text{H-NMR}$ analysis indicated that 55% of the amine groups in the IRMOF-3 framework were converted into amides calculated by comparing the areas of the $-\text{NH}_2$ between the modified and unmodified IRMOF-3. The thermal stability of IRMOF-3-LA and IRMOF-3-LA-Au was identical to that of IRMOF-3, with a major weight loss between $350\text{ }^\circ\text{C}$ and $500\text{ }^\circ\text{C}$ caused by decomposition of the organic linkers of the framework (Figure S3).

Figure 2 presents the H_2 -TPR profiles of the as-synthesized IRMOF-3-LA-Au and the recovered IRMOF-3-LA-Au after four cycles of A^3 coupling reaction at $80\text{ }^\circ\text{C}$ in the examined temperature range ($50\text{ }^\circ\text{C}$ – $500\text{ }^\circ\text{C}$). The TPR profiles of the as-synthesized IRMOF-3-LA-Au and recovered IRMOF-3-LA-Au exhibited two pronounced reduction peaks with the maximum in the range of $200\text{ }^\circ\text{C}$ – $250\text{ }^\circ\text{C}$ and $300\text{ }^\circ\text{C}$ – $410\text{ }^\circ\text{C}$, respectively. We have reported that the catalyst of $4.6\%\text{Au}/\text{IRMOF-3}$ showed two reduction peaks in the range of $190\text{ }^\circ\text{C}$ – $270\text{ }^\circ\text{C}$ and higher than $300\text{ }^\circ\text{C}$ that was attributed to the reduction of Au^{3+} to Au^0 and the decomposition of MOF, respectively¹⁷. Zhang *et al.* reported that the reduction temperature of Au^{3+} ions in IRMOF-3-SI-Au is $239\text{ }^\circ\text{C}$, higher than that of Au^{3+} ions supported on nanocrystalline CeO_2 ($107\text{ }^\circ\text{C}$) or on ZrO_2 ($210\text{ }^\circ\text{C}$)^{51–56}. Gil *et al.* reported that the TCD signals between $250\text{ }^\circ\text{C}$ and $377\text{ }^\circ\text{C}$ is mainly formed as consequence of the CO and CO_2 release resulting from the decomposition of carboxylic groups⁵⁷. Phan *et al.* reported that the peaks at $396\text{ }^\circ\text{C}$ and $415\text{ }^\circ\text{C}$ were attributed to the reduction of CuO structures formed during the total collapse of the $\text{Cu}_2(\text{BDC})_2(\text{DABCO})$ structure⁵⁸. Similar to a previous result, the H_2 -consumption peak observed at a low temperature range ($200\text{ }^\circ\text{C}$ – $250\text{ }^\circ\text{C}$) is attributed to the reduction of Au^{3+} ions into Au^0 nanoparticles⁵¹. The higher temperature peak is attributed to the decomposition of IRMOF-3⁵¹. The much lower intensities of the TCD signals of the recovered IRMOF-3-LA-Au after four successive cycles in the range of $200\text{ }^\circ\text{C}$ – $250\text{ }^\circ\text{C}$ than that for the as-synthesized IRMOF-3-LA-Au, suggesting a certain amount of Au^{3+} was reduced into Au^0 during A^3 coupling reaction.

Figure 3 shows the TEM images of the as-synthesized IRMOF-3-LA-Au and recovered IRMOF-3-LA-Au after four cycles of A^3 coupling reactions at $80\text{ }^\circ\text{C}$. Au^0 nanoparticles were not observed on the as-synthesized IRMOF-3-LA-Au, which is consistent with the XRD patterns of as-synthesized IRMOF-3-LA-Au. However, Au^0 nanoparticles with an average particle size of 3.0 nm were visible on the recovered IRMOF-3-LA-Au. This result is consistent with the H_2 -TPR results.

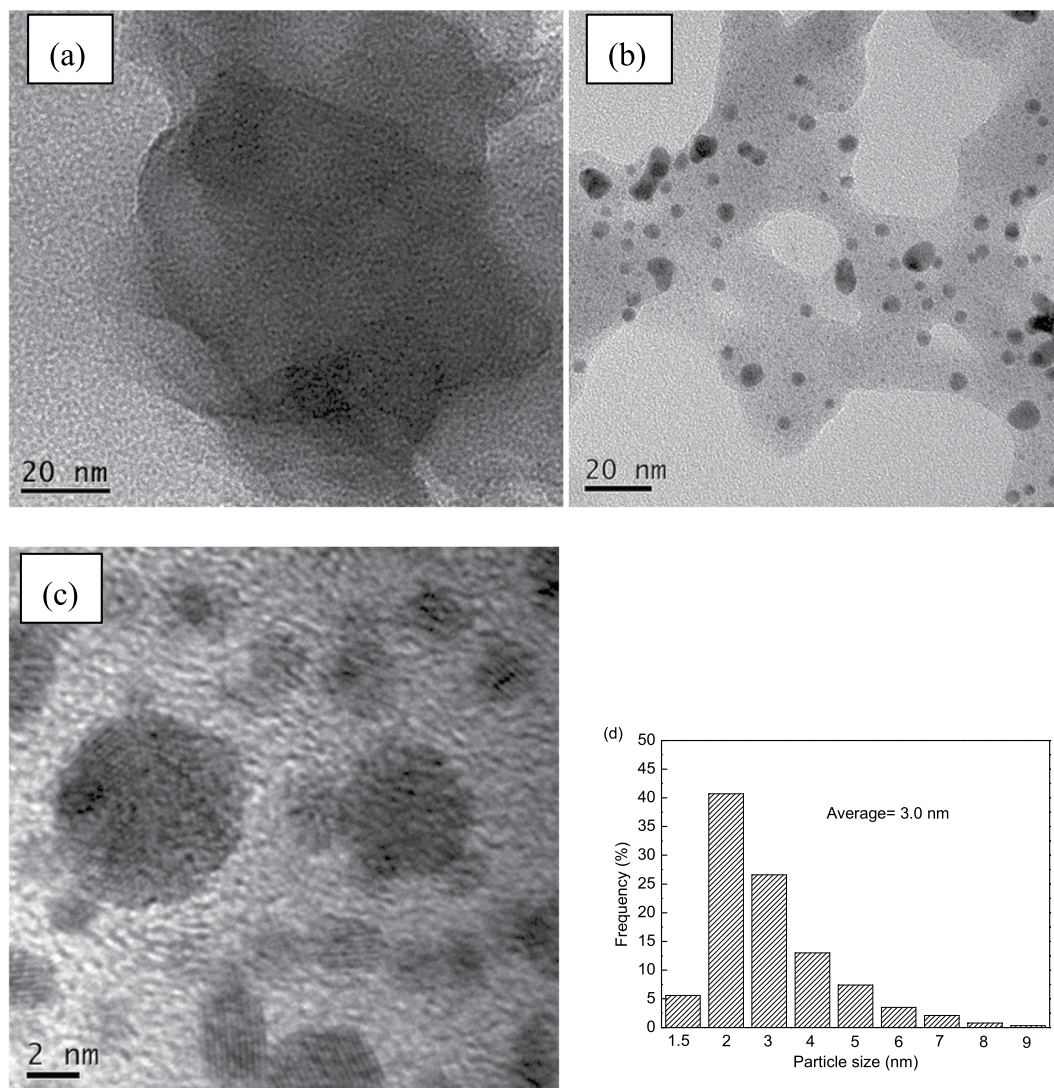


Figure 3. TEM image of as-synthesized IRMOF-3-LA-Au (a) and recovered IRMOF-3-LA-Au after four cycles of A³ coupling reactions at 80 °C (b and c), and the corresponding size distribution plot of Au nanoparticles (d).

Inductively coupled plasma atomic emission spectroscopy (ICP-AES) analysis indicated that the Au content of IRMOF-3-LA-Au was 4.9 wt% (0.2487 mmol/g), corresponding to 6.8% –NH₂ groups of IRMOF-3 having been functionalized. The loading of Au in recovered IRMOF-3-LA-Au after the four cycles of A³ coupling reactions at 80 °C was 4.1 wt% measured by ICP-AES. A large leaching of gold (ca. 16.3%) over the recovered IRMOF-3-LA-Au was observed as evidenced by ICP-AES.

Catalytic Tests. The prepared Au³⁺-containing catalysts with Au loading of 4.9 wt% on the MOF of IRMOF-3 were tested in the A³ coupling reaction. The reaction of benzaldehyde, phenylacetylene, and piperidine in a 1:1.2:1.3 mole ratio with 1,4-dioxane as solvent was selected as the model reaction. Given that temperature plays a crucial role in catalysis, the reaction was performed under varying reaction temperatures. Figure 4 shows the catalytic activity of IRMOF-3-LA-Au in the A³ coupling reaction of benzaldehyde, phenylacetylene, and piperidine at 80 °C, 100 °C, and 120 °C with 1,4-dioxane as solvent. IRMOF-3-LA-Au exhibited good catalytic activity in the A³ coupling reaction of benzaldehyde, phenylacetylene, and piperidine. The yield of propargylamines was 56% within 7 h at 80 °C. As temperature increased from 80 °C to 100 °C, the yield of propargylamines increased to 81% within 1 h. Further increase in temperature to 120 °C, a yield of 95% was obtained within 1 h. If one calculates the turnover number (TON) from the maximum yield taking into account the total Au content of the catalyst, the values obtained are 8, 12, and 14 for IRMOF-3-LA-Au at 80 °C, 100 °C, and 120 °C, respectively. In our previous work, maximum benzaldehyde conversion of 77% were obtained within 0.5 h at 120 °C over 4.6% Au/IRMOF-3 containing coexisting Au³⁺ ions and Au⁰ nanoparticles (Au³⁺/Au⁰ = 0.2)¹⁷. Au⁰ nanoparticles supported on IRMOF-3 yielded the desired propargylamines with a benzaldehyde conversion of 8% and 16% at 120 °C for 5 h over 0.6% Au/IRMOF-3 and 3.2% Au/IRMOF-3, respectively¹⁷. Taking into account the total Au content of the catalyst, the TON numbers from the maximum conversions were calculated to be 12, 9, and 4 for 4.6% Au/IRMOF-3, 0.6% Au/IRMOF-3, and 3.2% Au/IRMOF-3, respectively. Copper nanoparticles supported on

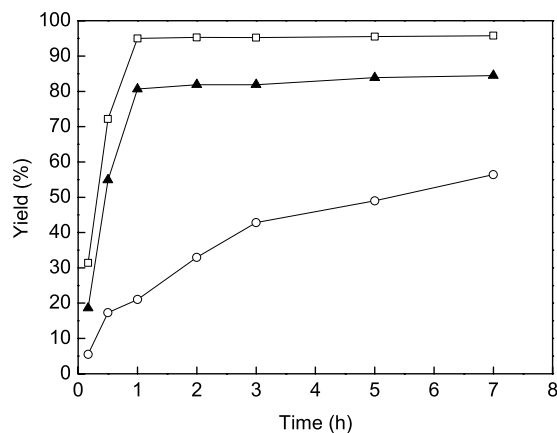
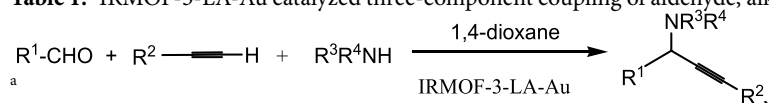


Figure 4. Comparison of catalytic activity for A^3 coupling reaction of benzaldehyde, phenylacetylene, and piperidine with 1,4-dioxane as solvent on IRMOF-3-LA-Au at 80 °C (open circle), 100 °C (triangle), and 120 °C (open square).

Entry	R ¹	R ²	R ³ R ⁴ NH	Temp./°C	Time/h	Yield/%
1	3-ClC ₆ H ₄	Ph	piperidine	80	7	35
2	3-ClC ₆ H ₄	Ph	piperidine	100	1	65
3	4-MeC ₆ H ₄	Ph	piperidine	80	7	54
4	4-MeC ₆ H ₄	Ph	piperidine	100	1	79
5	4-MeOC ₆ H ₄	Ph	piperidine	80	7	72
6	4-MeOC ₆ H ₄	Ph	piperidine	100	1	91
7	Cyclohexyl	Ph	piperidine	80	7	93
8	Heptyl	Ph	piperidine	80	7	94
9	Hexyl	Ph	piperidine	80	7	99
10	Ph	4-MeC ₆ H ₄	piperidine	80	7	65
11	Ph	4-MeC ₆ H ₄	piperidine	100	1	79
12	Ph	4-EtC ₆ H ₄	piperidine	80	7	54
13	Ph	4-EtC ₆ H ₄	piperidine	100	1	66
14	Ph	4-ButC ₆ H ₄	piperidine	80	7	31
15	Ph	4-ButC ₆ H ₄	piperidine	100	1	55
16	Ph	(CH ₃) ₃ Si	piperidine	80	7	72
17	Ph	(CH ₃) ₃ Si	piperidine	100	1	99
18	Ph	Hexyl	piperidine	100	1	25
19	Ph	Ph	morpholine	100	1	67
20	Ph	Ph	pyrrolidine	100	1	64
21	Ph	Ph	diethylamine	100	1	28

Table 1. IRMOF-3-LA-Au catalyzed three-component coupling of aldehyde, alkyne and amine^a.



Reaction conditions: aldehyde (0.25 mmol), amine (0.30 mmol), alkyne (0.33 mmol), IRMOF-3-LA-Au (0.07 g).

starch micro particles (CuNPs@MS) gave a yield of 30% within 20 h at 60 °C for the A^3 coupling reaction of benzaldehyde, phenylacetylene, and piperidine in 1,4-dioxane with a TON of 100 based on the total Cu content⁵⁹. NiO nanoparticles gave a yield of 95% at 120 °C for 22 h under N₂ atmosphere in toluene with a TON number of 6⁶⁰. Based on the above results, although the TON number of IRMOF-3-LA-Au is still less than those of CuNPs@MS, the catalyst of IRMOF-3-LA-Au shows higher activity than 4.6%Au/IRMOF-3, 0.6%Au/IRMOF-3, 3.2%Au/IRMOF-3, and NiO nanoparticles.

To demonstrate the generality of IRMOF-3-LA-Au as catalyst, the A^3 coupling of different combinations of aldehydes, alkynes, and amines were tested. First, we extended the reaction to various substituted benzaldehydes bearing electron-donating or electron-withdrawing groups (Table 1, entries 1–6). The coupling reaction with benzaldehyde bearing electron-donating groups, such as -CH₃ and -CH₃O, displayed higher yields than the

benzaldehyde bearing electron-withdrawing groups (Table 1, entries 1–6). In addition, reactions with aliphatic aldehydes, such as cyclohexanecarboxaldehyde, *n*-octyl aldehyde, and *n*-heptyl aldehyde also displayed good yield of propargylamines (Table 1, entries 7–9). Moreover, we attempted to expand the reaction to other alkynes, such as alkyl- and aryl-substituted terminal alkynes (Table 1, entries 10–18). The aromatic alkynes were also suitable substrates for A³ coupling reaction. The yield of propargylamines decreased with increasing the chain length of straight-chain alkyl substituted phenylacetylene (Table 1, entries 10–15). (Trimethylsilyl)acetylene also afforded propargylamines in good yields (Table 1, entries 16, 17). The yields of propargylamines reached to 72% and 99% at 80 °C and 100 °C, respectively. By contrast, 1-octyne afforded a 25% yield of propargylamines at 100 °C within 1 h. Furthermore, we investigated the scope of amines, including alicyclic and dialkyl amines (Table 1, entries 19–21). Reactions with alicyclic amines such as morpholine and pyrrolidine proceeded efficiently and resulted in moderate yield. However, the reaction proceeded slowly in the presence of dialkyl amine such as diethylamine with benzaldehyde and phenylacetylene to afford product in 28% yield.

The reusability studies of IRMOF-3-LA-Au were carried out on the A³ coupling reaction of benzaldehyde, phenylacetylene, and piperidine in 1,4-dioxane at 80 °C. The catalyst was recovered by separating IRMOF-3-LA-Au from the liquid component of the mixture via extensive centrifugation. The recovered catalyst was washed twice with 1,4-dioxane, dried at 50 °C under vacuum for 1 h, and reused. In four successive cycles, yields were 56%, 48%, 35%, and 26% at 80 °C for 7 h. The Au³⁺ species on the recovered IRMOF-3-LA-Au were reduced into Au⁰ during A³ coupling reaction as revealed by XRD, H₂-TPR and TEM results. The recovered IRMOF-3-LA-Au contains coexisting active centers: Au³⁺ ions and Au⁰ nanoparticles. Studies have reported that the activity of Au-based catalysts in A³ coupling reaction decreases in the following order: Au³⁺ > Au⁰^{51,61}. Therefore, reduction of Au³⁺ species is possibly one of the main reasons for the deactivation of IRMOF-3-LA-Au catalysts.

We performed a leaching test to examine if there are any homogeneous active species in solution that could catalyze the A³ coupling reaction^{62–66}. The hot filtration test was carried out by stopping the A³ coupling reaction of benzaldehyde, phenylacetylene, and piperidine after 2 h at 80 °C. The yield of propargylamines reached to 33% within 2 h at 80 °C. The reaction solution was removed quickly from the catalyst of IRMOF-3-LA-Au and was transferred to another reactor under the same reaction conditions. The yield of propargylamines increased to 37% after reaction another 2 h at 80 °C. These results demonstrate that there are some leaching active species under the reaction conditions. This result was confirmed by ICP-AES analysis of the recovered IRMOF-3-LA-Au after four reaction cycles which showed large leaching of Au species (16.3%) to reaction medium.

Conclusions

We successfully designed a new heterogeneous catalyst for A³ coupling reactions by anchoring Au³⁺ onto microporous IRMOF-3 via a postsynthetic modification method. IRMOF-3-LA-Au showed high catalytic activity for the A³ coupling reaction of aldehyde, alkyne, and amine in 1,4-dioxane. In addition, IRMOF-3-LA-Au is applicable for a wide range of substrates, including aromatic and aliphatic aldehydes, alkyl- and aryl-substituted terminal alkynes, and alicyclic amines. IRMOF-3-LA-Au can be easily separated from the mixture and can be reused for four cycles, thus making the catalyst highly desirable in addressing environmental concerns.

Methods

IRMOF-3 Preparation. IRMOF-3 was synthesized using a solvothermal method. In brief, 2-aminoterephthalic acid (NH₂-BDC, 0.3723 g, 2 mmol) and Zn(NO₃)₂·6H₂O (1.78 g, 7 mmol) were dissolved in 70 mL DMF and stirred for 30 min at room temperature. The mixture was subsequently transferred into a 100-milliliter Teflon Liner with a metallic Paar Bomb. The container was placed in an oven at 100 °C for 24 h to yield brown crystals. After cooling overnight, the mother liquor was decanted and the as-synthesized materials were washed with 3 × 20 mL of DMF and then with 3 × 20 mL of chloroform (CHCl₃). The product was dried at 50 °C for 12 h under vacuum before use^{17,67,68}.

IRMOF-3-LA Preparation. In a typical synthesis, freshly dried IRMOF-3 (0.3 g, 1.095 mmol eq of –NH₂) was dispersed in a 25 mL vial containing 10 mL of acetonitrile (CH₃CN). Lactic acid (3.83 mmol, 345.0 mg) was added with stirring (400 r/min), and the mixture was stirred under reflux for 3 h. The sample was collected by centrifugation and washed three times with CH₃CN (3 × 8 mL). The solid was then dried at 50 °C for 4 h under vacuum to yield the final compound, IRMOF-3-LA.

IRMOF-3-LA-Au Preparation. Gold functionalized IRMOF-3 was prepared via postsynthetic modification. HAuCl₄·4H₂O (0.052 g) was dissolved in CH₃CN (0.50 mL). HAuCl₄·4H₂O solution was subsequently added dropwise into the dried IRMOF-3 (0.50 g) at room temperature. The sample was stored overnight and dried at 50 °C for 3 h under vacuum.

Catalyst Characterization. XRD was performed with Bruker D8 diffractometer operated with a Cu K α radiation ($\lambda = 1.541 \text{ \AA}$) at 40 mA and 40 kV. Nitrogen physisorption measurements were carried out using a Quantachrome instrument at 77 K. Samples weighing 80–100 mg were outgassed for 12 h at 50 °C prior to measurement. FT-IR spectrum (400–4000 cm⁻¹) was recorded from KBr pellet in NICOLET 5700 FT-IR spectrometer. ¹H-NMR spectra were recorded on Bruker Advance III HD spectrometer (500 MHz). Approximately 5 mg of IRMOF-3 and IRMOF-3-LA samples were dried under vacuum at 90 °C for 12 h and digested with sonication in 500 μ L DMSO-*d*₆ and 100 μ L dilute DCl (23 μ L of 35% DCl in D₂O diluted with 1.0 mL of DMSO-*d*₆). Approximately 10–20 mg of IRMOF-3, IRMOF-3-LA, or IRMOF-3-LA-Au was used for TGA measurements. Samples were analyzed under a stream of N₂ using a TA SDT Q600 running from room temperature to 700 °C with a scan rate of 15 °C/min. ICP-AES analysis was performed on a Perkin-Elmer Optima 7000 DV apparatus. TEM studies were carried out with a FEI TECNAI F20 Transmission Electron Microscope. H₂-TPR was conducted on a ChemStar apparatus equipped with a TCD detector. A 50-milligram portion of each sample was

loaded in a U-shaped quartz microreactor and heated at a ramping rate of 10°C/min in 5 vol% H₂ in Ar (a total flow of 50 mL/min).

Catalytic Measurements. A mixture of IRMOF-3-LA-Au (70 mg, 0.0177 mmol Au), aldehyde (0.25 mmol), alkyne (0.33 mmol), amine (0.30 mmol), and 1,4-dioxane (1.5 mL) was placed in a closed glass reactor (8.0 mL, SYNTHWARE) and vigorously stirred at 80°C–120°C in an oil bath for 0.15–7 h. After the reaction was completed, the mixture was cooled to room temperature and centrifuged at 14000 rpm for 6 min. IRMOF-3-LA-Au was deposited into the bottom of a centrifuge tube and separated from the liquid component of the mixture. The liquid was analyzed using a GC (GC-1100, capillary column, SE-54).

References

- Abdoli, M., Saeidian, H. & Kakanejadifard, A. Highly efficient one-pot synthesis of novel propargylamine-based sulfonamides by an A³-coupling reaction. *Synlett* **27**, 2473–2476 (2016).
- Belluti, F. *et al.* Design, synthesis and anticancer activities of stilbene-coumarin hybrid compounds: identification of novel proapoptotic agents. *Bioorg. Med. Chem.* **18**, 3543–3550 (2010).
- León, R., García, A. G. & Marco-Contelles, J. Recent advances in the multitarget-directed ligands approach for the treatment of Alzheimer's disease. *Med. Res. Rev.* **33**, 139–189 (2013).
- Bolea, I., Gella, A. & Unzeta, M. Propargylamine-derived multitarget-directed ligands: fighting Alzheimer's disease with monoamine oxidase inhibitors. *J. Neural Transm.* **120**, 893–902 (2013).
- Mccormack, P. L. Rasagiline: a review of its use in the treatment of idiopathic Parkinson's disease. *CNS Drugs* **28**, 1083–1097 (2014).
- Hattori, G. *et al.* Copper-catalyzed enantioselective propargylic amination of propargylic esters with amines: copper-allenylidene complexes as key intermediates. *J. Am. Chem. Soc.* **132**, 10592–10608 (2010).
- Periasamy, M. *et al.* Diastereoselective synthesis of tetrasubstituted propargylamines via hydroamination and metalation of 1-alkynes and their enantioselective conversion to trisubstituted chiral allenes. *J. Org. Chem.* **81**, 987–999 (2016).
- Varyani, M., Khatri, P. K. & Jain, S. L. Amino acid ionic liquid bound copper Schiff base catalyzed highly efficient three component A³-coupling reaction. *Catal. Commun.* **77**, 113–117 (2016).
- Liu, L. L. *et al.* Catalysis by metal-organic frameworks: proline and gold functionalized MOFs for the aldol and three-component coupling reactions. *RSC Adv.* **4**, 13093–13107 (2014).
- Li, Z. H., Jiang, Z. J. & Su, W. K. Fast, solvent-free, highly enantioselective three-component coupling of aldehydes, alkynes, and amines catalyzed by the copper(II)pybox complex under high-vibration ball-milling. *Green Chem.* **17**, 2330–2334 (2015).
- Berrichi, A., Bachir, R., Benabdallah, M. & Choukchou-Braham, N. Supported nano gold catalyzed three-component coupling reactions of amines, dichloromethane and terminal alkynes (AHA). *Tetrahedron Lett.* **56**, 1302–1306 (2015).
- Borah, S. J. & Das, D. K. Modified montmorillonite clay stabilized silver nanoparticles: an active heterogeneous catalytic system for the synthesis of propargylamines. *Catal. Lett.* **146**, 656–665 (2016).
- Rahman, M., Bagdi, A. K., Majee, A. & Hajra, A. Nano indium oxide catalyzed efficient synthesis of propargylamines via C–H and C–Cl bond activations. *Tetrahedron Lett.* **52**, 4437–4439 (2011).
- Sharma, R., Sharma, S. & Gaba, G. Silica nanospheres supported diazafluorene iron complex: an efficient and versatile nanocatalyst for the synthesis of propargylamines from terminal alkynes, dihalomethane and amines. *RSC Adv.* **4**, 49198–49211 (2014).
- Periasamy, M. *et al.* Zinc salt promoted diastereoselective synthesis of chiral propargylamines using chiral piperazines and their enantioselective conversion into chiral allenes. *Eur. J. Org. Chem.* **2014**, 6067–6076 (2014).
- Samai, S., Nandi, G. C. & Singh, M. An efficient and facile one-pot synthesis of propargylamines by three-component coupling of aldehydes, amines, and alkynes via C–H activation catalyzed by NiCl₂. *Tetrahedron Lett.* **51**, 5555–5558 (2010).
- Liu, L. L., Zhang, X., Gao, J. S. & Xu, C. M. Engineering metal-organic frameworks immobilize gold catalysts for highly efficient one-pot synthesis of propargylamines. *Green Chem.* **14**, 1710–1720 (2012).
- Zhang, X. & Corma, A. Supported gold(III) catalysts for highly efficient three-component coupling reactions. *Angew. Chem. Int. Ed.* **47**, 4358–4361 (2008).
- Cole-Hamilton, D. J. Homogeneous catalysis—new approaches to catalyst separation, recovery, and recycling. *Science* **299**, 1702–1706 (2003).
- Corma, A., Iglesias, M., Xamena, F. X. L. I. & Sánchez, F. Cu and Au metal-organic frameworks bridge the gap between homogeneous and heterogeneous catalysts for alkene cyclopropanation reactions. *Chem. Eur. J.* **16**, 9789–9795 (2010).
- Rose, M. Nanoporous polymers: bridging the gap between molecular and solid catalysts? *ChemCatChem* **6**, 1166–1182 (2014).
- He, T. *et al.* A base-resistant Zn^{II}-based metal-organic framework: synthesis, structure, postsynthetic modification, and gas adsorption. *ChemPlusChem* **81**, 864–871 (2016).
- Mounfield, W. P. *et al.* Synergistic effect of mixed oxide on the adsorption of ammonia with metal-organic frameworks. *Ind. Eng. Chem. Res.* **55**, 6492–6500 (2016).
- Li, L. *et al.* Flexible metal-organic frameworks with discriminatory gate-opening effect for the separation of acetylene from ethylene/acetylene mixtures. *Eur. J. Inorg. Chem.* **2016**, 4457–4462 (2016).
- He, Y. *et al.* A microporous metal-organic framework for highly selective separation of acetylene, ethylene, and ethane from methane at room temperature. *Chemistry* **18**, 613–619 (2012).
- Gangu, K. K., Dadhich, A. S. & Mukkamala, S. B. Synthesis, crystal structure and fluorescent properties of two metal-organic frameworks constructed from Cd(II) and 2,6-naphthalene dicarboxylic acid. *Synth. React. Inorg. M.* **47**, 313–319 (2017).
- Schrimpf, W. *et al.* Investigation of the Co-dependence of morphology and fluorescence lifetime in a metal-organic framework. *Small* **12**, 3651–3657 (2016).
- Liu, L., Chen, X., Qiu, J. & Hao, C. New insights into the nitroaromatics-detection mechanism of the luminescent morganic framework sensor. *Dalton Trans.* **44**, 2897–2906 (2015).
- Cao, Y. Y., Guo, X. F. & Wang, H. High sensitive luminescence metal-organic framework sensor for hydrogen sulfide in aqueous solution: a trial of novel turn-on mechanism. *Sensor. Actuat. B-Chem.* **243**, 8–13 (2017).
- Zhu, C. F. *et al.* Chiral metal-organic framework as a platform for cooperative catalysis in asymmetric cyanosilylation of aldehydes. *ACS Catal.* **6**, 7590–7596 (2016).
- Cheng, S. S. *et al.* Efficient multicomponent synthesis of propargylamines catalyzed by copper nanoparticles supported on metal-organic framework derived nanoporous carbon. *Catal. Commun.* **89**, 91–95 (2017).
- Lian, X. & Yan, B. A postsynthetic modified MOF hybrid as heterogeneous photocatalyst for α -phenethyl alcohol and reusable fluorescence sensor. *Inorg. Chem.* **55**, 11831–11838 (2016).
- Tanabe, K. K. & Cohen, S. M. Engineering a metal-organic framework catalyst by using postsynthetic modification. *Angew. Chem. Int. Ed.* **48**, 7424–7427 (2009).
- Miao, Z. C., Qi, C., Wensley, A. M. & Luan, Y. Development of a novel Brønsted acid UiO-66 metal-organic framework catalyst by postsynthetic modification and its application in catalysis. *RSC Adv.* **6**, 67226–67231 (2016).
- Gee, W. J. *et al.* Furnishing amine-functionalized metal-organic frameworks with the β -amidoketone group by postsynthetic modification. *Inorg. Chem.* **55**, 10839–10842 (2016).

36. Liu, J., Zhang, X. B., Yang, J. & Wang, L. Postsynthetic modification of IRMOF-3 with a copper iminopyridine complex as heterogeneous catalyst for the synthesis of 2-aminobenzothiazoles. *Appl. Organometal. Chem.* **28**, 198–203 (2014).
37. Sun, Z. G., Li, G., Liu, H. O. & Liu, L. P. Salen-Co(II) complex incorporated into amino-functionalized MIL-101(Cr) through postsynthetic modification as a cooperative catalyst for cyclohexane selective oxidation. *Appl. Catal. A Gen.* **466**, 98–104 (2013).
38. Wang, Z., Tanabe, K. K. & Cohen, S. M. Accessing postsynthetic modification in a series of metal-organic frameworks and the influence of framework topology on reactivity. *Inorg. Chem.* **48**, 296–306 (2009).
39. Dietl, C. *et al.* Switch-on fluorescence of a perylene-dye-functionalized metal-organic framework through postsynthetic modification. *Chem. Eur. J.* **21**, 10714–10720 (2015).
40. Liu, B., Jie, S., Bu, Z. & Li, B. G. Postsynthetic modification of mixed-linker metal-organic frameworks for ethylene oligomerization. *RSC Adv.* **4**, 62343–62346 (2014).
41. Albert-Soriano, M. & Pastor, I. M. Metal-organic framework based on copper and carboxylate-imidazole as robust and effective catalyst in the oxidative amidation of carboxylic acids and formamides. *Eur. J. Org. Chem.* **2016**, 5180–5188 (2016).
42. Wittmann, T. *et al.* Enhancing the water stability of Al-MIL-101-NH₂ via postsynthetic modification. *Chem. Eur. J.* **21**, 314–323 (2015).
43. Candu, N. *et al.* Postsynthetic modification of a metal-organic framework (MOF) structure for enantioselective catalytic epoxidation. *ChemPlusChem* **78**, 443–450 (2013).
44. Tabatabaeian, K., Zanjanchi, M. A., Mahmoodi, N. O. & Eftekhari, T. Anchorage of a ruthenium complex into modified MOF: synergistic effects for selective oxidation of aromatic and heteroaromatic compounds. *RSC Adv.* **5**, 101013–101022 (2015).
45. Lee, Y. R. *et al.* Facile synthesis of an IRMOF-3 membrane on porous Al₂O₃ substrate via a sonochemical route. *Micropor. Mesopor. Mat.* **213**, 161–168 (2015).
46. Nguyen, J. G. & Cohen, S. M. Moisture-resistant and superhydrophobic metal-organic frameworks obtained *via* postsynthetic modification. *J. Am. Chem. Soc.* **132**, 4560–4561 (2010).
47. Kaye, S. S., Dailly, A., Yaghi, O. M. & Long, J. R. Impact of preparation and handling on the hydrogen storage properties of Zn₄O(1,4-benzenedicarboxylate)₃ (MOF-5). *J. Am. Chem. Soc.* **129**, 14176–14177 (2007).
48. Liu, L. L. *et al.* Supported Au/MOF-5: a highly active catalyst for three-component coupling reactions. *CISEC Journal* **66**, 1738–1747 (2015).
49. Li, D. *et al.* Morphology design of IRMOF-3 crystal by coordination modulation. *Cryst. Growth Des.* **14**, 5856–5864 (2014).
50. Wang, X. L. *et al.* Adsorptive removal of sulfur compounds using IRMOF-3 at ambient temperature. *Appl. Surf. Sci.* **289**, 107–113 (2014).
51. Zhang, X., Xamena, F. X. L. I. & Corma, A. Gold(III)-metal organic framework bridges the gap between homogeneous and heterogeneous gold catalysts. *J. Catal.* **265**, 155–160 (2009).
52. Concepcion, P., Carretin, S. & Corma, A. Stabilization of cationic gold species on Au/CeO₂ catalysts under working conditions. *Appl. Catal. A Gen.* **307**, 42–45 (2006).
53. Guzman, J., Carretin, S. & Corma, A. Spectroscopic evidence for the supply of reactive oxygen during CO oxidation catalyzed by gold supported on nanocrystalline CeO₂. *J. Am. Chem. Soc.* **127**, 3286–3287 (2005).
54. Zhang, X., Shi, H. & Xu, B. Q. Catalysis by gold: isolated surface Au³⁺ ions are active sites for selective hydrogenation of 1,3-butadiene over Au/ZrO₂ catalysts. *Angew. Chem. Int. Ed.* **44**, 7132–7135 (2005).
55. Zhang, X., Shi, H. & Xu, B. Q. Comparative study of Au/ZrO₂ catalysts in CO oxidation and 1,3-butadiene hydrogenation. *Catal. Today* **122**, 330–337 (2007).
56. Liu, Z. P., Wang, C. M. & Fan, K. N. Single gold atoms in heterogeneous catalysis: Selective 1,3-butadiene hydrogenation over Au/ZrO₂. *Angew. Chem. Int. Ed.* **45**, 6865–6868 (2006).
57. Gil, S. *et al.* Nano-scale Au supported on carbon materials for the low temperature water gas shift (WGS) reaction. *Catalysts* **1**, 155–174 (2011).
58. Phan, N. T., Nguyen, T. T., Nguyen, V. T. & Nguyen, K. D. Ligand-free copper-catalyzed coupling of phenols with nitroarenes by using a metal-organic framework as a robust and recoverable catalyst. *ChemCatChem* **5**, 1–9 (2013).
59. Gholinejad, M., Saadati, F., Shaybanizadeh, S. & Pullithadathil, B. Copper nanoparticles supported on starch micro particles as a degradable heterogeneous catalyst for three-component coupling synthesis of propargylamines. *RSC Adv.* **6**, 4983–4991 (2016).
60. Gajengi, A. L., Sasaki, T. & Bhanage, B. M. NiO nanoparticles catalyzed three component coupling reaction of aldehyde, amine and terminal alkynes. *Catal. Commun.* **72**, 174–179 (2015).
61. Liu, L. L. *et al.* Supported Au/MIL-53(Al): a reusable green solid catalyst for the three-component coupling reaction of aldehyde, alkyne, and amine. *Reac. Kinet. Mech. Cat.* **119**, 335–348 (2016).
62. Guo, Z. *et al.* Pt nanoclusters confined within metal-organic framework cavities for chemoselective cinnamaldehyde hydrogenation. *ACS Catal.* **4**, 1340–1348 (2014).
63. Li, X. *et al.* Tandem catalysis by palladium nanoclusters encapsulated in metal-organic frameworks. *ACS Catal.* **4**, 3490–3497 (2014).
64. Li, X. *et al.* Controlling catalytic properties of Pd nanoclusters through their chemical environment at the atomic level using isorecticular metal-organic frameworks. *ACS Catal.* **6**, 3461–3468 (2016).
65. Chen, Y. Z. *et al.* Multifunctional PdAg@MIL-101 for one-pot cascade reactions: combination of host-guest cooperation and bimetallic synergy in catalysis. *ACS Catal.* **5**, 2062–2069 (2015).
66. Li, X. *et al.* Impact of linker engineering on the catalytic activity of metal-organic frameworks containing Pd(II)-bipyridine complexes. *ACS Catal.* **6**, 6324–6328 (2016).
67. Tanabe, K. K., Wang, Z. & Cohen, S. M. Systematic functionalization of a metal-organic framework via a postsynthetic modification approach. *J. Am. Chem. Soc.* **130**, 8508–8517 (2008).
68. Eddaoudi, M. *et al.* Systematic design of pore size and functionality in isorecticular MOFs and their application in methane storage. *Science* **295**, 469–472 (2002).

Acknowledgements

We gratefully acknowledge the funding by the National Natural Science Foundation of China (21171132), the Promotive Research Fund for Young and Middle-aged Scientists of Shandong Province (BS2014CL021), the Project of Shandong Province Higher Educational Science and Technology Program (J14LC01), the Technology Research and Development Program of Weifang (2014GX030, 2016GX013), and Science Foundation of Weifang University.

Author Contributions

L.L. and X.T. designed the study. L.L. performed experiments. L.L., X.T., X.Z., C.X., and Y.Y. analyzed the data. L.L. and X.Z. wrote the manuscript. X.T. and C.X. revised the manuscript. All authors reviewed the manuscript.

Additional Information

Supplementary information accompanies this paper at <https://doi.org/10.1038/s41598-017-13081-0>.

Competing Interests: The authors declare that they have no competing interests.

Publisher's note: Springer Nature remains neutral with regard to jurisdictional claims in published maps and institutional affiliations.



Open Access This article is licensed under a Creative Commons Attribution 4.0 International License, which permits use, sharing, adaptation, distribution and reproduction in any medium or format, as long as you give appropriate credit to the original author(s) and the source, provide a link to the Creative Commons license, and indicate if changes were made. The images or other third party material in this article are included in the article's Creative Commons license, unless indicated otherwise in a credit line to the material. If material is not included in the article's Creative Commons license and your intended use is not permitted by statutory regulation or exceeds the permitted use, you will need to obtain permission directly from the copyright holder. To view a copy of this license, visit <http://creativecommons.org/licenses/by/4.0/>.

© The Author(s) 2017